scientific reports

Check for updates

OPEN

Tunable optical nonreciprocity in double-cavity optomechanical system with nonreciprocal coupling

Mian Mao, Hongmei Jiang, Cui Kong✉ & Jibing Liu

We propose a double-cavity optomechanical system with nonreciprocal coupling to realize tunable optical nonreciprocity that has the prospect of making an optical device for the manipulation of information processing and communication. Here we investigate the steady-state dynamic processes of the double-cavity system and the transmission of optical waves from opposite cavity directions. The transmission spectrum of the probe field is presented in detail and the physical mechanism of the induced transparency window is analyzed. It is found that the nonreciprocal response of the probe field transmission appears at two different coupling strengths between two cavities, which breaks the spatial symmetry to lead to optical nonreciprocal transmission. In addition, through analytical calculations, we have given the conditions for nonreciprocal effects, and the optimally nonreciprocal effects can be controlled by adjusting both the coupling strengths and the dissipation rates of cavity fields. Due to the simplicity of the device, this study may provide promising opportunities to realize nonreciprocal structures for optical wave transmission.

Cavity optomechanics, as a unique platform to explore the radiation-pressure interaction, has attracted extensive experimental and theoretical interests owing to its wide applications in various classical and quantum information processing, weak signal measurement, and development of new devices[1–7]. All kinds of optomechanical systems have been proposed and manufactured to research abundant physical phenomena and applications, such as entanglements[8–10], optomechanical chaos[11,12], high-order sideband generation[13–17], cooling of mechanical oscillators[18–20], optomechanically induced transparency (OMIT)[21–25]. Due to the sharp transmission features of OMIT regulated by the control laser beam, it makes many applications ranging from force sensor to quantum communication possible. In recent years, except for the simple cavity optomechanical systems, various hybrid optomechanical systems have been proposed to study OMIT in numerous different physical mechanisms, such as parity-time symmetric OMIT[26,27], nonlinear OMIT[28,29] and double OMIT[30,31]. Compared to the conventional OMIT, double and multiple OMIT[32] own many favorable features except multichannel transparency windows, including extensive integration and performance. Moreover, OMIT in integrated resonators provides us with a practical method for achieving optical nonreciprocity.

Optical nonreciprocity is a phenomenon in some devices that only allows optical signals to be transmitted in one direction, but prevents their transmission in the opposite direction, which is essential in a wide range of applications such as stealth or noiseless information processing. In the early days, breaking reciprocity or time-reversal symmetry is usually achieved through the magneto-optical effects[33–35], but its disadvantage were large, high cost, and not suitable for on-chip integration. With the development of nanophotonics as well as the improvement of nano-fabrication techniques, non-magnetic approaches for realizing optical nonreciprocity have been extensively studied with significant advances, such as nonlinear effect[36–38], parametric modulation[39–41] and optomechanical coupling[42–46]. Until now, nonreciprocal effects have been studied extensively in the context of optomechanical systems, such as by tuning the phase difference between the two optomechanical coupling rates to breaking the time-reversal symmetry of the system[47,48], by optically pumping the ring resonator[49] or by resonant Brillouin scattering[50,51] to enhance the optomechanical coupling in one direction and suppress in the other one, by breaking of the algebraic duality symmetry[52] to give rise to different behaviors between the forward and the backward transmissions, and so on.

In this paper, a scheme about optical nonreciprocal phenomena in a double-cavity optomechanical system with nonreciprocal coupling is proposed. First, we investigate the steady-state dynamic processes of the double-cavity system in the red-detuning regime by using the perturbation method. We find that the system gives rise to bistability due to the strong optomechanical interaction driven by the control field, and the coupling strengths between two cavities have a regulating effect on the number of photons, which plays an important role in the

College of Physics and Electronic Science, Hubei Normal University, Huangshi 435002, P. R. China. ✉email: cuikong@hbnu.edu.cn

subsequent study of optical nonreciprocal transmission. Second, we show the transmission spectrum of the probe field and analyze the physical mechanism of the induced transparency windows in detail. It is found that the coupling strengths play a decisive role in the nonreciprocal response of the probe field transmission, which breaks the spatial symmetry to lead to optical nonreciprocal transmission. Finally, the effects of the parameters including the coupling strengths and the dissipation rates of cavity fields on the nonreciprocal response of the system are discussed numerically, and with selecting the appropriate parameters, we can achieve tunable optical nonreciprocity. The theoretical scheme to realize optical nonreciprocal transmission in double-cavity optomechanical systems provides a theoretical basis for applications of optical circulators, isolators and directional amplifiers and so on.

The paper is organized as follows. In Sec. 2, we describe the model of the double-cavity optomechanical system and present the corresponding Hamiltonian. Based on the Hamiltonian, we introduce the linearization of the optomechanical interaction, and give the steady state of optomechanical dynamics. In Sec. 3, we show the transmission spectrum of the probe field with different characteristics, and discuss the optical nonreciprocity adjusting by both the coupling strengths and the dissipation rates of cavity fields. In Sec. 4, a conclusion of the results is summarized.

Theoretical model and equations

Here, we study the optical nonreciprocal transmission based on the optomechanically induced transparency in a double-cavity optomechanical system. As shown in Fig. 1, we consider the two cavities consisting of an optomechanical cavity and an empty cavity. It is worth noting that the coupling strength between two cavities in our proposal is nonreciprocal ($\lambda_1 \neq \lambda_2$), which can be achieved by making use of an imaginary gauge field[53,54], impurity[55], or an auxiliary nonreciprocal transition device[56–59]. In addition, we provide a possible method for achieving nonreciprocal coupling in the Appendix 5. We demonstrate that coupling two cavities to a common additional mode and adiabatic elimination of the additional mode can result in the unequal coupling ($\lambda_1 \neq \lambda_2$) expressed in Eq.(1). The double-cavity optomechanical system is driven by a strong control field with frequency ω_c input from cavity a_1, and two weak probe fields with frequency ω_p input from both cavity a_1 and cavity a_2. In case one (as forward direction), the probe field is only input from cavity a_1, and the output field is obtained from cavity a_2. In case two (as backward direction), the probe field is only input from cavity a_2 and the output field is obtained from cavity a_1. We will next study the anti-Stokes field (probe field) output from the two opposite directions. The total Hamiltonian of the system can be written as follows[60]:

$$\begin{aligned}\hat{H} =&\hbar\omega_1\hat{a}_1^\dagger\hat{a}_1 + \hbar\omega_2\hat{a}_2^\dagger\hat{a}_2 + \hbar\omega_m\hat{b}^\dagger\hat{b} + \hbar\lambda_1\hat{a}_1^\dagger\hat{a}_2 + \hbar\lambda_2\hat{a}_1\hat{a}_2{}^\dagger \\ &- \hbar g\hat{a}_1^\dagger\hat{a}_1(\hat{b}^\dagger + \hat{b}) + \hat{H}_{driven},\end{aligned} \tag{1}$$

where $\hat{a}_{1,2}$ ($\hat{a}_{1,2}^\dagger$) indicates the annihilation (creation) operator of the cavity mode with resonance frequency $\omega_{1,2}$, and $\hat{b}$ ($\hat{b}^\dagger$) denotes the annihilation (creation) operator of the mechanical oscillator mode with vibration frequency ω_m. λ_1 and λ_2 are the coupling strengths between the two optical cavities respectively, and g is the single photon coupling rate. $\hat{H}_{driven}$ is the driving term, and in case one , $\hat{H}_{driven} = i\hbar\sqrt{\eta_1\kappa_1}\varepsilon_c(\hat{a}_1^\dagger e^{-i\omega_c t} - \hat{a}_1 e^{i\omega_c t}) + i\hbar\sqrt{\eta_1\kappa_1}\varepsilon_p(\hat{a}_1^\dagger e^{-i\omega_p t} - \hat{a}_1 e^{i\omega_p t})$, and in case two, $\hat{H}_{driven} = i\hbar\sqrt{\eta_1\kappa_1}\varepsilon_c(\hat{a}_1^\dagger e^{-i\omega_c t} - \hat{a}_1 e^{i\omega_c t}) + i\hbar\sqrt{\eta_2\kappa_2}\varepsilon_p(\hat{a}_2^\dagger e^{-i\omega_p t} - \hat{a}_2 e^{i\omega_p t})$. The amplitudes of the control field and the probe field are $\varepsilon_c = \sqrt{\mathrm{P_c}/\hbar\omega_c}$ and $\varepsilon_p = \sqrt{\mathrm{P_p}/\hbar\omega_p}$, respectively, where $\mathrm{P_c}$ is the power of the control field, and $\mathrm{P_p}$ is the power of the probe field. κ_1 and κ_2 are the total dissipation rates of cavity a_1 and cavity a_2. We have furthermore used the coupling parameter $\eta_{1,2} \equiv \kappa_{ex}/(\kappa_o + \kappa_{ex})$ where κ_o denotes the intrinsic loss rate, which depends on the Q factor of the cavity and κ_{ex} is the external loss rate (i.e. wave guide coupling). Experimentally, the parameter $\eta_{1,2}$ can be continuously adjusted by tuning the taper-resonator gap[61]. Here the coupling parameter is chosen to be the critical coupling 1/2[21].

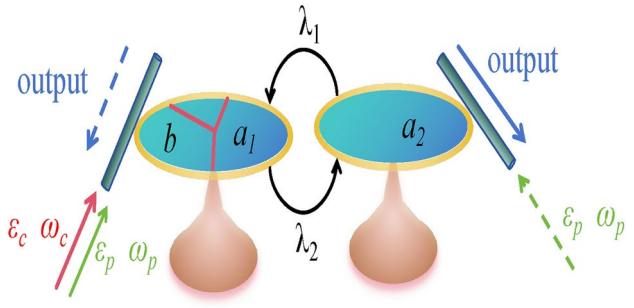

Fig. 1. Schematic of a double-cavity optomechanical system that consists of two cavities, in which one of cavities combines with a mechanical oscillator to form an optomechanical cavity. The coupling strengths between the two cavities represent λ_1 and λ_2. The system is driven by a strong control field with frequency ω_c input from cavity a_1, and two weak probe fields with frequency ω_p input from both cavity a_1 and cavity a_2.

In the rotating frame of the frequency ω_c, by introducing the dissipations, the dynamic behavior of the system can be described by the following Heisenberg-Langevin equations:

$$\begin{aligned}\dot{\hat{a}}_1 =&[-i\Delta_1 + ig(\hat{b}^\dagger + \hat{b}) - \kappa_1/2]\hat{a}_1 - i\lambda_1\hat{a}_2 \\ &+ \sqrt{\kappa_1/2}(\varepsilon_c + \varepsilon_p e^{-i\Omega t}) + \sqrt{\kappa_1/2}\hat{a}_{1.\mathrm{in}},\end{aligned} \tag{2}$$

$$\begin{aligned}\dot{\hat{a}}_2 =&(-i\Delta_2 - \kappa_2/2)\hat{a}_2 - i\lambda_2\hat{a}_1 + \sqrt{\kappa_2/2}\varepsilon_p e^{-i\Omega t} \\ &+ \sqrt{\kappa_2/2}\hat{a}_{2.\mathrm{in}},\end{aligned} \tag{3}$$

$$\dot{\hat{b}} =(-i\omega_m - \gamma_m/2)\hat{b} + ig\hat{a}_1^\dagger\hat{a}_1 + \sqrt{\gamma_m/2}\hat{b}_{\mathrm{in}}, \tag{4}$$

where $\Delta_i = \omega_i - \omega_c (i = 1, 2)$ is the frequency detuning of the control field from the cavity field, and $\Omega = \omega_p - \omega_c$ is the frequency detuning of the control field from the probe field. The dissipation rate of the mechanical oscillator is γ_m. In addition, $\hat{a}_{1.\mathrm{in}}$, $\hat{a}_{2.\mathrm{in}}$, and $\hat{b}_{\mathrm{in}}$ represent the quantum noise of the two cavity fields and the thermal noise of the mechanical oscillator, respectively, and they are characterized by the following temperature-dependent correlation functions: $\langle\hat{a}_{1.\mathrm{in}}(t)\hat{a}_{1.\mathrm{in}}^\dagger(t')\rangle = [n_{th}(\omega_1) + 1]\delta(t - t')$, $\langle\hat{a}_{1.\mathrm{in}}^\dagger(t)\hat{a}_{1.\mathrm{in}}(t')\rangle = [n_{th}(\omega_1)]\delta(t - t')$, $\langle\hat{a}_{2.\mathrm{in}}(t)\hat{a}_{2.\mathrm{in}}^\dagger(t')\rangle = [n_{th}(\omega_2) + 1]\delta(t - t')$, $\langle\hat{a}_{2.\mathrm{in}}^\dagger(t)\hat{a}_{2.\mathrm{in}}(t')\rangle = [n_{th}(\omega_2)]\delta(t - t')$, $\langle\hat{b}_{\mathrm{in}}(t)\hat{b}_{\mathrm{in}}^\dagger(t')\rangle = [b_{th}(\omega_m) + 1]\delta(t - t')$, $\langle\hat{b}_{\mathrm{in}}^\dagger(t)\hat{b}_{\mathrm{in}}(t')\rangle = [b_{th}(\omega_m)]\delta(t - t')$. Here, $n_{th}(\omega_{1,2}) = [\exp(\frac{\hbar\omega_{1,2}}{K_B T}) - 1]^{-1}$ and $b_{th}(\omega_m) = [\exp(\frac{\hbar\omega_m}{K_B T}) - 1]^{-1}$ are the equilibrium average thermal photon and phonon number respectively, where K_B is the Boltzmann constant and T is the ambient temperature.

In this work, we focus on the mean response of the system, and thus the evolution of the system operators can be reduced to their expectation values, viz. $\langle\hat{a}_1\rangle = a_1$, $\langle\hat{a}_2\rangle = a_2$, $\langle\hat{b}\rangle = b$. Moreover, the quantum and thermal noise terms ($\langle\hat{a}_{1.\mathrm{in}}(t)\rangle$, $\langle\hat{a}_{2.\mathrm{in}}(t)\rangle$, $\langle\hat{b}_{\mathrm{in}}(t)\rangle$) can be dropped safely because their expectation values are zero in the semiclassical approximation. Therefore, the mean value equations can be further written as follows:

$$\begin{aligned}\dot{a}_1 =&[-i\Delta_1 + ig(b^* + b) - \kappa_1/2]a_1 - i\lambda_1 a_2 \\ &+ \sqrt{\kappa_1/2}(\varepsilon_c + \varepsilon_p e^{-i\Omega t}),\end{aligned} \tag{5}$$

$$\dot{a}_2 =(-i\Delta_2 - \kappa_2/2)a_2 - i\lambda_2 a_1 + \sqrt{\kappa_2/2}\varepsilon_p e^{-i\Omega t}, \tag{6}$$

$$\dot{b} =(-i\omega_m - \gamma_m/2)b + iga_1^* a_1. \tag{7}$$

Here, we consider the control field is significantly stronger than the probe field, and thus the perturbation approach can be used to deal with the above equations of motion. The influence of the control field on the system can be regarded as a steady state, and the probe field is treated as a perturbation of the steady state due to the relatively weak probe field. Based on this research method, we can reformulate the operators as: $a_{1,2} = \bar{a}_{1,2} + \delta a_{1,2}$, $a_{1,2}^* = \bar{a}_{1,2}^* + \delta a_{1,2}^*$, $b = \bar{b} + \delta b$, $b^* = \bar{b}^* + \delta b^*$. By substituting the redefined operators into Eqs. (5)-(7), the steady-state solutions of the system can be obtained as:

$$\bar{a}_1 =\frac{i\lambda_1\bar{a}_2 - \sqrt{\kappa_1/2}\varepsilon_c}{-i\Delta_1 + ig(\bar{b}^* + \bar{b}) - \kappa_1/2}, \tag{8}$$

$$\bar{a}_2 =\frac{i\lambda_2\bar{a}_1}{-i\Delta_2 - \kappa_2/2}, \tag{9}$$

$$\bar{b} =\frac{ig\bar{a}_1^*\bar{a}_1}{i\omega_m + \gamma_m/2}. \tag{10}$$

According to Eqs.(8-10), we have a third-order nonlinear equation for the photon number $|\bar{a}_1|^2$,

$$t_3|\bar{a}_1|^6 + t_2|\bar{a}_1|^4 + t_1|\bar{a}_1|^2 - d_1 = 0, \tag{11}$$

with

$$t_3 =g^4\omega_m^2(\Delta_2^2 + \kappa_2^2), \tag{12}$$

$$t_2 =2g^2\omega_m(\omega_m^2 + \gamma_m^2/4)[2(\varsigma + \lambda_1\lambda_2)\Delta_2 - \beta\kappa_2], \tag{13}$$

$$t_1 =[(\varsigma + \lambda_1\lambda_2)^2 + \beta^2](\omega_m^2 + \gamma_m^2/4)^2, \tag{14}$$

$$d_1 =(\omega_m^2 + \gamma_m^2/4)^2(\Delta_2^2 + \kappa_2^2/4)\kappa_1\varepsilon_c^2/2, \tag{15}$$

in which $\varsigma = \kappa_1\kappa_2/4 + J^2 - \Delta_1\Delta_2$, $\beta = \Delta_1\kappa_2/2 + \Delta_2\kappa_1/2$. In this way, we can easily obtain the photon number $|\bar{a}_1|^2$, and further obtain the photon number $|\bar{a}_2|^2$ and the phonon number $|\bar{b}|^2$.

Through the above Eqs.(8-10), we find that the coupling strengths λ_1 and λ_2 between the two cavities are closely related to the photon number of the two cavities. Then, we plot Fig. 2 to show the steady-state average photon number $|\bar{a}_1|^2$ varies with the power P_c of the control field and the coupling strength λ_1. It is obvious that the steady-state photon number $|\bar{a}_1|^2$ increases with the increase of the power of the control field, and when the power reaches the range of around 1.95 mW to 5.08 mW, three solutions exist and the middle part is an unstable solution, where the system gives rise to bistability in this case. The result is consistent with the bistable properties[22] caused by the optomechanical interation in a general optomechanical system. In addition, it is found that when the power is small, the coupling strength λ_1 has almost no modulation effect on the photon number, but with the increase of the power, the coupling strength begins to modulate the number of photons. The coupling strength λ_2 has a similar regulatory function. Here, we focus on the low-excitation regime where the control field is too weak to induce bistability (the power of the control field is kept below 1.95 mW throughout the analysis to avoid any bistability in the system).

Next, we further consider the perturbations generated by the probe field on the system. Submitting the expressions $a_{1,2} = \bar{a}_{1,2} + \delta a_{1,2}$, $a^*_{1,2} = \bar{a}^*_{1,2} + \delta a^*_{1,2}$, $b = \bar{b} + \delta b$, $b^* = \bar{b}^* + \delta b^*$ into Eqs. (5)-(7), the equations of fluctuation terms can be written as:

$$\begin{aligned}\frac{d}{dt}\delta a_1 =&[-i\Delta_1 + ig(\bar{b}^* + \bar{b}) - \kappa_1/2]\delta a_1 - i\lambda_1\delta a_2 \\ &+ ig(\delta b^* + \delta b)(\bar{a}_1 + \delta a_1) + \sqrt{\kappa_1/2}\varepsilon_p e^{-i\Omega t},\end{aligned} \tag{16}$$

$$\frac{d}{dt}\delta a_2 =(-i\Delta_2 - \kappa_2/2)\delta a_2 - i\lambda_2\delta a_1 + \sqrt{\kappa_2/2}\varepsilon_p e^{-i\Omega t}, \tag{17}$$

$$\frac{d}{dt}\delta b =(-i\omega_m - \gamma_m/2)\delta b + ig(\bar{a}^*_1\delta a_1 + \bar{a}_1\delta a^*_1 + \delta a_1\delta a^*_1). \tag{18}$$

When we consider the nonlinear terms $ig(\delta b^* + \delta b)\delta a_1$ and $ig\delta a_1\delta a^*_1$, some interesting effects appear, one of which is a series of spectroscopic sideband with frequency $\omega_c \pm n\Omega$. In this work, we mainly focus on the first-order sideband generation, and the spectral components of second-order and high-order sidebands are ignored, so the perturbation solutions can be further ansatz as: $\delta a_1 = A^- e^{-i\Omega t} + A^+ e^{i\Omega t}$, $\delta a_2 = B^- e^{-i\Omega t} + B^+ e^{i\Omega t}$, $\delta b = C^- e^{-i\Omega t} + C^+ e^{i\Omega t}$, where $\Omega = \omega_p - \omega_c$. The frequency components with $-\Omega$ and $+\Omega$ represent the upper and lower first-order sideband generation, respectively, corresponding to the anti-Stokes field and Stokes field. In what follows, we solve Eqs. (16)-(18) by using above ansatz and give the amplitudes of the first-order sideband, leading to six algebraic equations:

$$(-i\Omega - \Theta)A^- =ig[C^- + (C^+)^*]\bar{a}_1 - i\lambda_1 B^- + \sqrt{\kappa_1/2}\varepsilon_p, \tag{19}$$

$$(i\Omega - \Theta)A^+ =ig[C^+ + (C^-)^*]\bar{a}_1 - i\lambda_1 B^+, \tag{20}$$

$$(-i\Omega - D)B^- = -i\lambda_2 A^- + \sqrt{\kappa_2/2}\varepsilon_p, \tag{21}$$

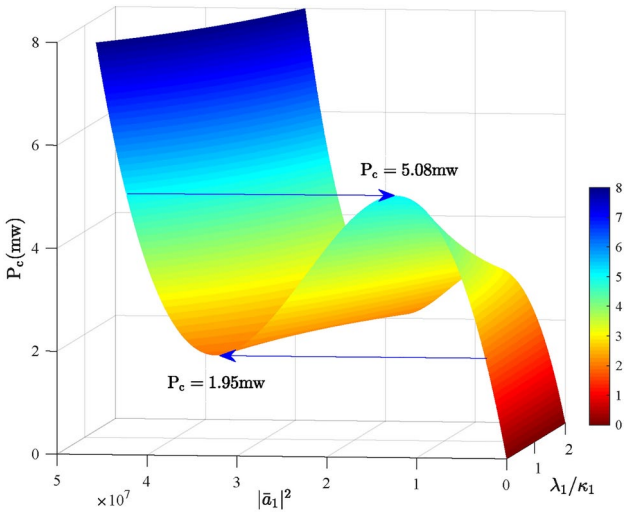

Fig. 2. Three dimensional functional diagram of coupling strength λ_1, pump power P_c and average photon number $|\bar{a}_1|^2$ of cavity a_1. The parameters are $\lambda_2 = \lambda_1$, $\gamma_m/2\pi = 410$ KHz, $\kappa_1/2\pi = 50$ MHz, $\omega_m/2\pi = 100$ MHz, $g = 1.2 \times 10^{-4}\omega_m$, $\Delta_1 = \Delta_2 = \Omega = \omega_m$, $\kappa_2 = \kappa_1$ and $\varepsilon_p = 0.05\varepsilon_c$, which are adopted from recent relevant studies[62] and are available in the experiments.

$$(i\Omega - D)B^{+} = -i\lambda_2 A^{+}, \tag{22}$$

$$(-i\Omega - E)C^{-} = ig[A^{-}\bar{a}_1^{*} + (A^{+})^{*}\bar{a}_1], \tag{23}$$

$$(i\Omega - E)C^{+} = ig[A^{+}\bar{a}_1^{*} + (A^{-})^{*}\bar{a}_1], \tag{24}$$

where $\Theta = -i\Delta_1 + ig(\bar{b}^{*} + \bar{b}) - \kappa_1/2$, $D = -i\Delta_2 - \kappa_2/2$, $E = -i\omega_m - \gamma_m/2$. $A^{\pm}$ represents the amplitude of the lower (upper) first-order sideband of cavity a_1; $B^{\pm}$ represents the amplitude of the lower (upper) first-order sideband of cavity a_2 and $C^{\pm}$ represents the amplitude of the lower (upper) first-order sideband of the mechanical oscillator. In order to study the optical response of light transmission when the probe field enters the cavity field from two opposite directions (forward and backward directions), we divide them into two cases in the following discussion:

In case one (as forward direction), the probe field is input from the left cavity a_1 and we study the optical response output from right cavity a_2. Here A_1^{-} represents the amplitude of the upper first-order sideband of cavity a_1, and B_1^{-} represents the amplitude of the upper first-order sideband of cavity a_2. The sideband amplitudes in this case can be obtained by solving Eqs.(19-24) where $\sqrt{\kappa_2/2}\varepsilon_p$ is dropped:

$$A_1^{-} = \frac{\Lambda Q(i\Omega + D)\sqrt{\kappa_1/2}\varepsilon_p}{\Lambda\Xi - 4\omega_m^2 g^4 |\bar{a}_1|^4 (i\Omega + D)(-i\Omega - D^{*})}, \tag{25}$$

$$B_1^{-} = \frac{i\Lambda Q\lambda_2\sqrt{\kappa_1/2}\varepsilon_p}{\Lambda\Xi - 4\omega_m^2 g^4 |\bar{a}_1|^4 (i\Omega + D)(-i\Omega - D^{*})}, \tag{26}$$

where $Q = (\gamma_m/2 - i\Omega)^2 + \omega_m^2$, $\Xi = Q(-i\Omega - \Theta)(i\Omega + D) - Q\lambda_1\lambda_2 - 2i\omega_m g^2|\bar{a}_1|^2(i\Omega + D)$, $\Lambda = Q(-i\Omega - \Theta^{*})(-i\Omega - D^{*}) + Q\lambda_1\lambda_2 + 2i\omega_m g^2|\bar{a}_1|^2(-i\Omega - D^{*})$.

In case two (as backward direction), the probe field is input from the right cavity a_2 and we study the optical response output from left cavity a_1. Here A_2^{-} represents the amplitude of the upper first-order sideband of cavity a_1, and B_2^{-} represents the amplitude of the upper first-order sideband of cavity a_2. The sideband amplitudes in this case can also be obtained by solving Eqs.(19-24) where $\sqrt{\kappa_1/2}\varepsilon_p$ is dropped:

$$A_2^{-} = \frac{i\Lambda Q\lambda_1\sqrt{\kappa_2/2}\varepsilon_p}{\Lambda\Xi - 4\omega_m^2 g^4 |\bar{a}_1|^4 (i\Omega + D)(-i\Omega - D^{*})}, \tag{27}$$

$$\begin{aligned} B_2^{-} = &-\sqrt{\kappa_2/2}\varepsilon_p(i\Omega + D) \\ &- \frac{\Lambda Q\lambda_1\lambda_2(i\Omega + D)\sqrt{\kappa_2/2}\varepsilon_p}{\Lambda\Xi - 4\omega_m^2 g^4 |\bar{a}_1|^4 (i\Omega + D)(-i\Omega - D^{*})}. \end{aligned} \tag{28}$$

According to the standard input-output notation[63,64], the total output in the forward and backward directions (in case one and in case two) at the probe field frequency ω_p can be obtained as:

$$c_{p_1} = -\sqrt{\kappa_1/2}B_1^{-}, \tag{29}$$

$$c_{p_2} = -\sqrt{\kappa_2/2}A_2^{-}. \tag{30}$$

In addition, we define t_{p_1} and t_{p_2} as the corresponding transmission amplitudes:

$$t_{p_1} = \frac{c_{p_1}}{\varepsilon_p},\ t_{p_2} = \frac{c_{p_2}}{\varepsilon_p}. \tag{31}$$

Here $|t_{p_1}|^2$ and $|t_{p_2}|^2$ are dimensionless, as the efficiency of the upper first-order sideband (the probe field) process. In what follows, we will present a detailed discussion of the transmission characteristics of the probe field.

The features of optical nonreciprocal transmission

In this section, we discuss in detail the transmission characteristics of the probe field output from cavity a_2 (in case one) and cavity a_1 (in case two). The transmission efficiency $|t_{p_1}|^2$ and $|t_{p_2}|^2$ of the probe field as a function of the driven frequency Ω/ω_m are shown in Fig. 3 under different coupling strengths (λ_1 and λ_2) and powers P_c of the control field. When the coupling strength is weak, seeing in Fig. 3(a) ($\lambda_1 = \lambda_2 = 0.4\kappa_1$), a Lorentzian curve appears in the transmission spectrum of the probe field. The Lorentzian peak in the transmission spectrum represents an absorption of the probe field, because the transmission amplitude is actually the case of

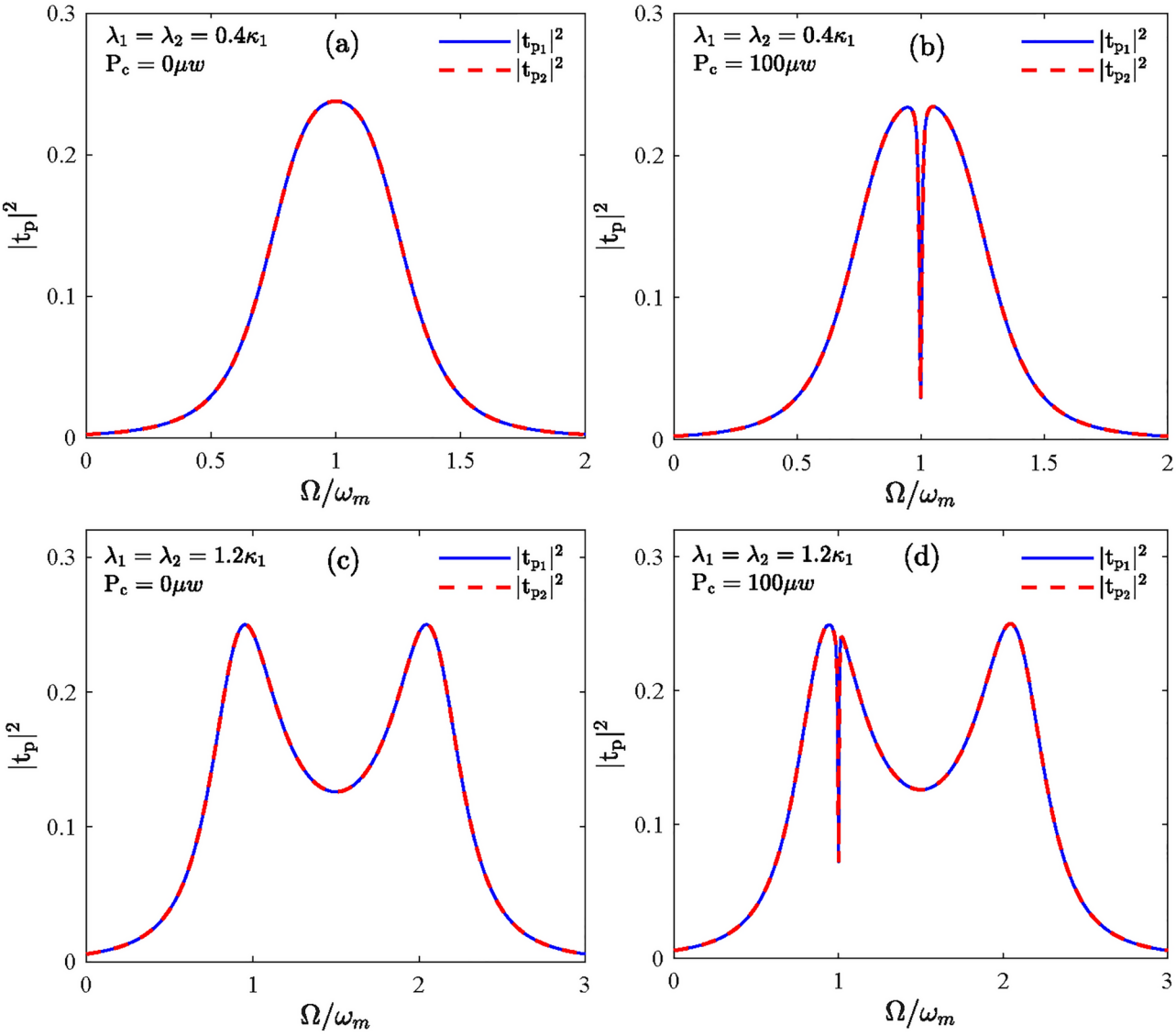

Fig. 3. Calculation results of $|t_p|^2$ (including $|t_{p_1}|^2$ and $|t_{p_2}|^2$) are plotted as functions of Ω/ω_m under different powers P_c and coupling strengths λ (including λ_1 and λ_2). We use $\Delta_1 = \Delta_2 = 1.5\omega_m$ in panels (c) and (d), and the other parameters are the same as in Fig. 2.

the probe field in the cavity. However, by increasing the coupling strength to $1.2\kappa_1$, a transparency window with a certain width (a dip corresponds to a transparent window) starts appearing, as shown in Fig. 3(c). The reason for the result is that the strong coupling strength of two cavities leads to the splitting of the two cavity modes, thus forming two absorption points (two peaks presented in this work). Moreover, the transparency dip of the transmission spectrum of the probe field will increase with increasing the coupling strength.

When we consider the driving field (control field) applied to the optomechanical cavity, the effective optomechanical coupling constant g begins to play a major role in the probe field transmission process, as shown in Fig. 3b, where the power of the control field is 100 μW. It is found that there is a transparent window near the resonance condition $\Omega = \omega_m$, and as the power increases, the transparent window will be more obvious and much deeper, which is similar to the contents of previous studies[22]. Its physical essence is that when the resonant condition of the mechanical oscillator is the same as that of the cavity, the destructive interference between the input probe field and the sideband excitations of the control field occurs, leading to a tunable transparent window. Therefore, the transparent windows in Figs. 3(b) and 3(c) are caused by different physical mechanisms. Further, when we use $\lambda_1 = \lambda_2 = 1.2\kappa_1$ and $P_c = 100$ μW in Fig. 3d, the result was predictable that there are double transparent windows, one of which is induced due to the strong coupling strength of two cavities, and the other of which is caused by the effective optomechanical interaction.

In order to investigate the nonreciprocal transmission of the probe field along two opposite directions, we plot Fig. 4. Based on Figs. 3(b), 3(c), and 3(d), we have only changed κ_2 to $0.5\kappa_1$ in Figs. 4(a), 4(b), and 4(c). In contrast to Fig. 3, Fig. 4 shows obvious nonreciprocal transmissions of the probe field, but upon closer

inspection, there are no significant change in the overall graphical characteristics. From the point of view of the transmission amplitudes, the value of $|t_{p_1}|^2$ is significantly increased, while the value of $|t_{p_2}|^2$ is relatively reduced. For example, when $\Omega = \omega_m$, the amplitudes of both $|t_{p_1}|^2$ and $|t_{p_2}|^2$ are about 0.03 in Fig. 3(b), but the amplitude of $|t_{p_1}|^2$ is 0.09 and the amplitude of $|t_{p_2}|^2$ is about 0.02 in Fig. 4(a), which shows a clearly nonreciprocal response of the probe field transmission. Especially for the comparison of Fig. 3(c) and Fig. 4(b), in the absence of the optomechanical interaction ($P_c = 0\ \mu W$), the optical nonreciprocal transmission is also obtained by changing the dissipation rate of cavity a_2. This indicates the algebraic duality symmetry does not rely on the specific optomechanical interaction. However, the drawback is that in Figs. 4(a), 4(b) and 4(c), although we can intuitively see the difference between the amplitudes of $|t_{p_1}|^2$ and $|t_{p_2}|^2$, the ratio of the amplitude difference does not change with the change of the driven frequency Ω/ω_m, that is to say, Ω/ω_m can not modulate the optical nonreciprocal transmission.

We define a dimensionless quantity I to describe the optical nonreciprocal transmission in the optomechanical system:

$$\mathrm{I} = 10\left|\log_{10}\frac{|t_{p_1}|^2}{|t_{p_2}|^2}\right| = 10\left|\log_{10}\frac{|c_{p_1}|^2}{|c_{p_2}|^2}\right|, \tag{32}$$

where the unit of I is dB. We label the dimensionless quantity I as the isolation rate to describe the degree of nonreciprocal transmission of the forward and backward input of the probe field. By judging the value of I,

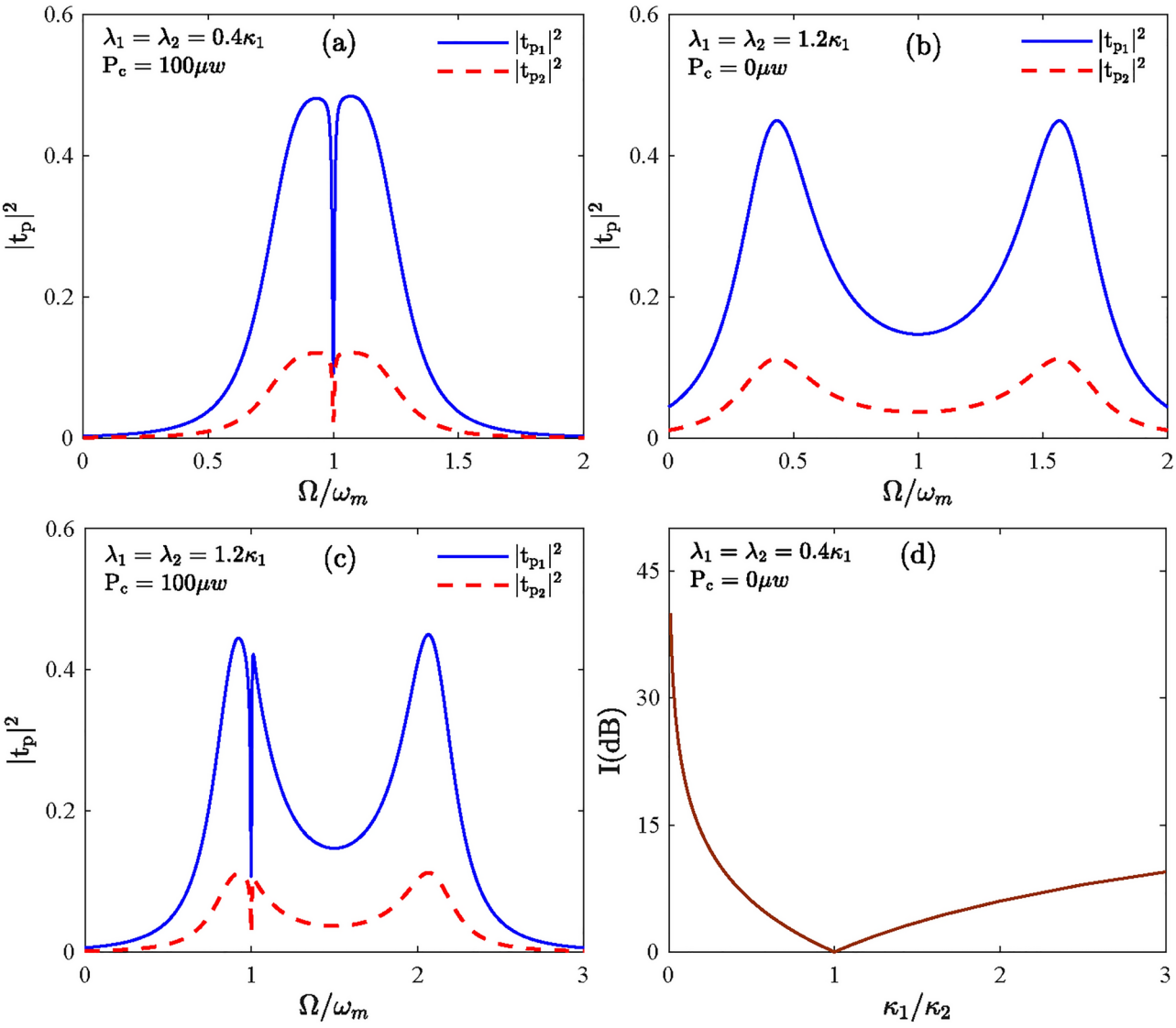

Fig. 4. The transmission efficiency $|t_{p_1}|^2$ (blue solid curve) and $|t_{p_2}|^2$ (red dashed curve) are plotted as functions of the Ω/ω_m under different powers P_c and coupling strengths λ (including λ_1 and λ_2) in panels (**a**), (**b**) and (**c**) with $\kappa_2 = 0.5\kappa_1$. In panel (**d**), the isolation ratio I of the probe field nonreciprocal transmission is plotted as a function of the κ_1/κ_2. The other parameters are the same as in Fig. 3.

we can determine the degree of the optical nonreciprocal transmission. When $|t_{p1}|^2/|t_{p2}|^2 = 1$, that is $\mathrm{I} = 0$, indicating that the transmission of first-order sidebands (the probe field output) in two opposite directions is reciprocal. Conversely, a nonzero I presents the optical nonreciprocal transmission, and the greater the value of I the higher the degree of nonreciprocity of the transmission. For example, $\mathrm{I} \geq 1$, the transmission coefficient in one direction is at least 10 times that of the other direction, which indicates a strong nonreciprocity in the optical transmission along two opposite directions. By substituting Eq. (31) into Eq. (32), then the isolation rate can be further simplified as:

$$\mathrm{I} = 10\left|2\log_{10}\frac{\kappa_1\lambda_2}{\kappa_2\lambda_1}\right|. \tag{33}$$

According to Eq. (33), we find that the isolation rate is independent of the driven frequency Ω/ω_m, but related to the coupling strengths and the dissipation rates of cavity fields. Therefore, in Figs. 4(a), 4(b), and 4(c) it can be found that the nonreciprocal transmission of the probe field occurs, but the corresponding isolation rate remains constant with the change in frequency, because the dissipation rate changes only once. For the sake of further observing the influence of the dissipation rates on the isolation rate, we draw Fig. 4(d) to show the value of I as functions of the κ_1/κ_2. It can be observed that the isolation rate I varies linearly with the dissipation rate κ_1/κ_2 . When $\lambda_1 = \lambda_2 = 0.4\kappa_1$ in Fig. 4(d), the value of I becomes $10\left|2\log_{10}\frac{\kappa_1}{\kappa_2}\right|$, which is perfectly consistent with the evolution of image features. Especially when the value κ_1/κ_2 is smaller, not only the value of I is significantly improved, but also it enables us to obtain a high isolation rate (> 20 dB)[65].

On the basis of Eq. (33), we can know that in addition to the dissipation rates of cavity fields, the coupling strengths λ_1 and λ_2 between two cavities also affect the nonreciprocal transmission of the probe field. We give the numerical simulation of the transmission efficiency in Fig. 5, with different λ_2. We make the power value 0 μ W in Fig. 5, and therefore, the curve formed in the figure has nothing to do with the optomechanical interaction. When $\lambda_1 = 0.4\kappa_1$ and $\lambda_2 = 0.5\kappa_1$ in Fig. 5(a), there are two Lorentz curve lines. Using Eq. (33), the value of I becomes $10\left|2\log_{10}\frac{\lambda_2}{\lambda_1}\right|$, and once λ_2 is unequal to λ_1, $\mathrm{I} \neq 0$. These two transmission curves are inevitably unequal, as shown in Fig. 5(a). With the increase of λ_2, the amplitude value of the transmission efficiency $|t_{p1}|^2$ remains increasing, as shown in Figs. 5(b), 5(c), 5(d), and when the value of λ_2 reaches $1.2\kappa_1$ in Fig. 5(c), the blue solid curve due to the strong coupling strength begins to split sharply and a transparent window is formed. However, the amplitude value of the transmission efficiency $|t_{p2}|^2$ does not change much because the coupling strength λ_1 keeps constant. The variation of these two curves with respect to the coupling strengths can be concluded from Eqs. (26)-(27). Such a result can also be seen in Fig. 5(d). According to the above exhibition of the nonreciprocal transmission of the probe field regulated by the frequency detuning Ω/ω_m shown in Figs. 4 and 5, it is found that the essentially achieving non-reciprocity originates from the the dissipation rates of cavity fields and the coupling strengths between two cavities. If you want to realize the optical nonreciprocal transmission modulated by the frequency detuning $\Delta_1 - \Delta_2$, it is needed to study the transmission of steady-state photon number[52]. In this work, we consider the transmission of the probe field under the linear effect of the optomechanical interaction, so the frequency detunings Ω/ω_m and $\Delta_1 - \Delta_2$ have no regulating effect on the nonreciprocal transmission.

Therefore, for the sake of achieving the regulation of nonreciprocal transmission, we try to change other variables, i.e., the coupling strengths (λ_1 and λ_2). Figure 6 shows the isolation ratio I of the probe field nonreciprocal transmission as a function of the coupling strengths λ_1 and λ_2. As shown the yellow color parts in Fig. 6, the smaller the value of λ_1 or λ_2, the greater the value of the isolation rate I. In order to effectively raise the isolation ratio I of the optical nonreciprocal transmission, we make κ_2 equal to 0.5 times κ_1, or we can increase the ratio further. According to Eq. (33), the value of I here becomes $10\left|2\log_{10}\frac{2\lambda_2}{\lambda_1}\right|$, so the value of I is still a linear relationship to the ratio between λ_2 and λ_1. When λ_2 is equal to 0.5 times λ_1, $\mathrm{I} = 0$, as shown by the black line in the figure, indicating reciprocal transmission. However, as the ratio of λ_1 to λ_2 increases, we can obtain a high isolation rate I, which is clearly shown in the small plot in Fig. 6. This is the same as the result in Fig. 4 (d), since the isolation rate is linear with the coupling strengths and the dissipation rates, and with appropriate parameter selection, the isolation ratio I of optical nonreciprocal transmission can be significantly improved.

Conclusions

In summary, we study the optical nonreciprocal transmission of the probe field in a double-cavity optomechanical system with nonreciprocal coupling, and find that the tunable optical nonreciprocity can be obtained by adjusting the dissipation rates of cavity fields and the coupling strengths between two cavities. Using the linearization of the Heisenberg-Langevin equations, we have discussed the steady-state dynamic behavior of the system, and shown the transmission spectrum of the probe field with different characteristics, and their corresponding physical interpretation is also given. There are two different types of transparent windows, one of which is due to strong coupling strengths and the other is due to the optomechanical interaction. It is found that the dissipation rates and the coupling strengths play a decisive role in the optical nonreciprocal transmission, which is exactly consistent with the results of theoretical calculations. The greater the ratio of $\kappa_1\lambda_2$ to $\kappa_2\lambda_1$, the higher the

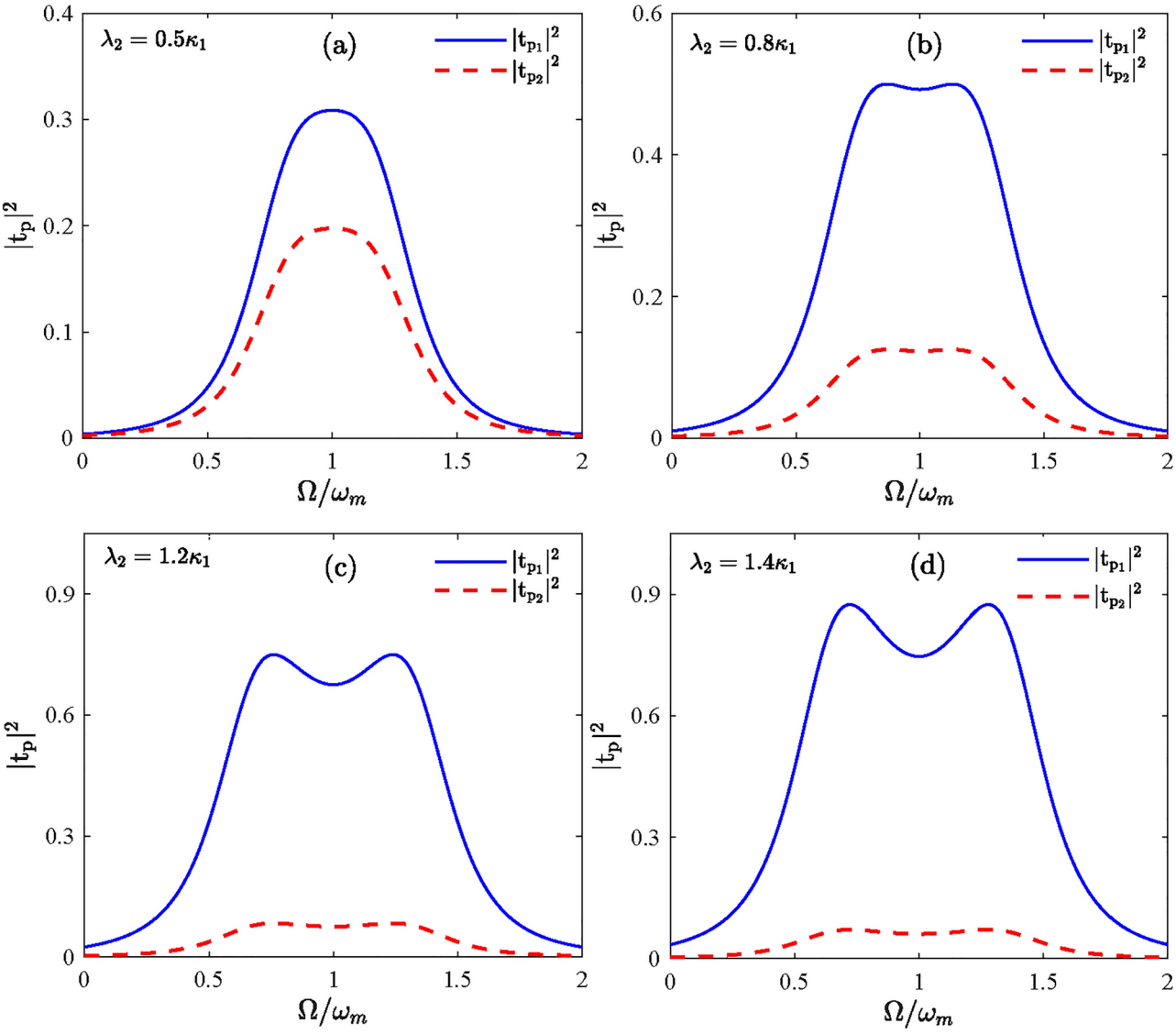

Fig.5. The transmission efficiency $|t_{p_1}|^2$ (blue solid curve) and $|t_{p_2}|^2$ (red dashed curve) are plotted as functions of the Ω/ω_m under different coupling strengths λ_2. We use $\mathrm{P_c} = 0\mu$W, $\lambda_1 = 0.4\kappa_1$, and the other parameters are the same as in Fig. 2.

isolation rate I obtained. The weak tunability of the driven frequency Ω/ω_m is the disadvantage of the present mechanism, which can be transformed by studying the steady-state photon number. The double-cavity system with nonreciprocal coupling has been proposed in many other studies[60] and we hope that this theoretical study can provide some guidance for the construction of non-reciprocal devices, such as optical isolators, diodes, and transducers.

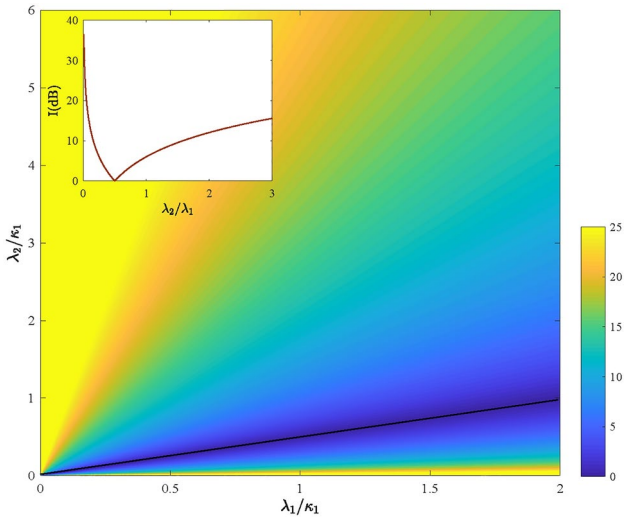

Fig. 6. The isolation ratio I of the probe field nonreciprocal transmission is plotted as a function of the coupling strengths λ_1 and λ_2. We use $P_c = 0\mu W$, $\kappa_2 = 0.5\kappa_1$, and the other parameters are the same as in Fig. 2.

Data availability

The datasets used and/or analysed during the current study available from the corresponding author on reasonable request.

A. The implementation of two cavity modes with nonreciprocal coupling

Here, we assume that there are three modes a_1, a_2, and m. Eliminating the m mode by adiabatic approximation, we can obtain that the coupling of a_1 mode and a_2 mode is nonreciprocal.
In this sense, the original Hamiltonian can be written as follows ($\hbar = 1$):

$$\begin{aligned}\hat{H} =&\omega_1\hat{a}_1^\dagger\hat{a}_1 + \omega_2\hat{a}_2^\dagger\hat{a}_2 + \omega_m\hat{m}^\dagger\hat{m} + (G\hat{a}_1^\dagger\hat{a}_2 + G^*\hat{a}_1\hat{a}_2^\dagger)\\ &+ G_1\hat{a}_1^\dagger\hat{m} + G_1^*\hat{a}_1\hat{m}^\dagger + G_2\hat{a}_2^\dagger\hat{m} + G_2^*\hat{a}_2\hat{m}^\dagger.\end{aligned} \tag{1}$$

The dynamic behavior of the system can be described by the following Heisenberg-Langevin equations:

$$\dot{a}_1 =(-i\omega_1 - \kappa_1/2)a_1 - iGa_2 - iG_1m + \sqrt{\kappa_1}a_{1,in}, \tag{2}$$

$$\dot{a}_2 =(-i\omega_2 - \kappa_2/2)a_2 - iG^*a_1 - iG_2m + \sqrt{\kappa_2}a_{2,in}, \tag{3}$$

$$\dot{m} =(-i\omega_m - \kappa_m/2)a_1 - iG_1^*a_1 - iG_2^*a_2 + \sqrt{\kappa_m}m_{in}. \tag{4}$$

Eq.(4) can be derived as:

$$\begin{aligned}m(t) =&e^{(-i\omega_m-\kappa_m/2)t}m(0) + e^{(-i\omega_m-\kappa_m/2)t}\\ &\cdot\int_0^t[-iG_1^*a_1(\tau) - iG_2^*a_2(\tau) + \sqrt{\kappa_m}m_{in}(\tau)]e^{(i\omega_m+\kappa_m/2)\tau}d\tau.\end{aligned} \tag{5}$$

Under conditions of large dissipation ($\kappa_m \gg \{\kappa_1, \kappa_2\}$), it can be obtained $e^{(-i\omega_m-\kappa_m/2)t} = 0$. So Eq.(5) can be further written as:

$$\begin{aligned}m(t) =&e^{(-i\omega_m-\kappa_m/2)t}[-iG_1^*a_1 - iG_2^*a_2 + \sqrt{\kappa_m}m_{in}]\int_0^t e^{(i\omega_m+\kappa_m/2)\tau}d\tau\\ =&\frac{-iG_1^*a_1 - iG_2^*a_2 + \sqrt{\kappa_m}m_{in}}{i\omega_m + \kappa_m/2}.\end{aligned} \tag{6}$$

Substitute Eq.(6) into Eqs.(2)and (3), respectively:

$$\begin{aligned}\dot{a}_1 =&[-i\omega_1 - \kappa_1/2 - \frac{|G_1|^2}{i\omega_m + \kappa_m/2}]a_1 - i\lambda_1a_2\\ &+ \sqrt{\kappa_1}a_{1,in} + \frac{iG_1\sqrt{\kappa_m}}{i\omega_m + \kappa_m/2}m_{in},\end{aligned} \tag{7}$$

$$\begin{aligned}\dot{a}_2 =&[-i\omega_2 - \kappa_2/2 - \frac{|G_2|^2}{i\omega_m + \kappa_m/2}]a_2 - i\lambda_2 a_1 \\ &+ \sqrt{\kappa_2}a_{2,in} + \frac{-iG_2\sqrt{\kappa_m}}{i\omega_m + \kappa_m/2}m_{in},\end{aligned} \tag{8}$$

where

$$\begin{aligned}\lambda_1 =&G + \frac{-iG_1G_2^*}{i\omega_m + \kappa_m/2} = G + \frac{e^{-i\frac{\pi}{2}}|G_1|e^{-i\theta_1}|G_2|e^{i\theta_2}}{\sqrt{\omega_m^2 + \kappa_m^2/4}e^{i\varphi}} \\ =&G + \frac{|G_1G_2|}{\sqrt{\omega_m^2 + \kappa_m^2/4}}e^{i(-\theta_1+\theta_2-\frac{\pi}{2}-\varphi)},\end{aligned} \tag{9}$$

and

$$\begin{aligned}\lambda_2 =&G^* + \frac{-iG_1^*G_2}{i\omega_m + \kappa_m/2} = G^* + \frac{e^{-i\frac{\pi}{2}}|G_1|e^{i\theta_1}|G_2|e^{-i\theta_2}}{\sqrt{\omega_m^2 + \kappa_m^2/4}e^{i\varphi}} \\ =&G + \frac{|G_1G_2|}{\sqrt{\omega_m^2 + \kappa_m^2/4}}e^{i(\theta_1-\theta_2-\frac{\pi}{2}-\varphi)}.\end{aligned} \tag{10}$$

Here, we assume G is a real number, and $\tan\varphi = \frac{2\omega_m}{\kappa_m}$. We set $\theta_1 - \theta_2 = \theta$, when

$$\begin{cases} -\theta - \frac{\pi}{2} - \varphi = (2k_1+1)\pi, & k_1 \in Z \\ \theta - \frac{\pi}{2} - \varphi = 2k_2\pi. & k_2 \in Z \end{cases} \tag{11}$$

If we assume $\theta = \frac{\pi}{2}$ and $\varphi = 0$, Eq.(9) can be simplified to

$$\lambda_1 = G - \frac{|G_1G_2|}{\sqrt{\omega_m^2 + \kappa_m^2/4}}, \tag{12}$$

and similarly, Eq.(10) can also be further reduced to

$$\lambda_2 = G + \frac{|G_1G_2|}{\sqrt{\omega_m^2 + \kappa_m^2/4}}. \tag{13}$$

Consequently, from Eqs.(12) and (13), it can be deduced that $\lambda_1 \neq \lambda_2$.

Received: 16 October 2024; Accepted: 21 January 2025
Published online: 27 January 2025

References

1. Aspelmeyer, M., Kippenberg, T. J. & Marquardt, F. Cavity Optomechanics. *Rev. Mod. Phys.* **86**, 1391–452 (2014).
2. Clerk, A. A., Devoret, M. H., Girvin, S. M., Marquardt, F. & Schoelkopf, R. J. Introduction to quantum noise, measurement, and amplification. *Rev. Mod. Phys.* **82**, 1155 (2010).
3. Tsang, M. & Caves, C. M. Coherent quantum-noise cancellation for optomechanical sensors. *Phys. Rev. Lett.* **105**, 123601 (2010).
4. Xiong, H. & Si, L. Precision measurement of electrical charges in an optomechanical system beyond linearized dynamics. *Appl. Phys. Lett.* **110**, 171102 (2017).
5. Safavi-Naeini, A. H. & Painter, O. Proposal for an optomechanical traveling wave phonon-photon translator. *New J. Phys.* **13**, 013017 (2011).
6. Teufel, J. D., Harlow, J. W., Regal, C. A. & Lehnert, K. W. Dynamical Backaction of Microwave fields on a Nanomechanical Oscillator. *Phys. Rev. Lett.* **101**, 197203 (2008).
7. Liao, J. Q. & Tian, L. Macroscopic Quantum Superposition in Cavity Optomechanics. *Phys. Rev. Lett.* **116**, 163602 (2016).
8. Liao, J. Q., Wu, Q. Q. & Nori, F. Entangling two macroscopic mechanical mirrors in a two-cavity optomechanical system. *Phys. Rev. A* **89**(1), 014302 (2014).
9. Lü, X. Y., Zhu, G. L., Zheng, L. L. & Wu, Y. Entanglement and quantum superposition induced by a single photon. *Phys. Rev. A* **97**(3), 033807 (2018).
10. Jiang, C. et al. Switchable Bipartite and Genuine Tripartite Entanglement via an Optoelectromechanical Interface. *Phys. Rev. A* **101**, 042320 (2020).
11. Monifi, F. et al. Optomechanically induced stochastic resonance and chaos transfer between optical fields. *Nat. Photon.* **10**, 399 (2016).
12. Zhu, G. L., Hu, C. S. & Wu, Y. Lü, X. *Y. Cavity Optomech. chaos. Fundamental Res.* **3**(1), 63–74 (2023).
13. Liu, Z.-X., Xiong, H. & Wu, Y. Generation and amplification of a high-order sideband induced by two-level atoms in a hybrid optomechanical system. *Phys. Rev. A* **97**(1), 013801 (2018).
14. Kong, C., Xiong, H. & Wu, Y. Coulomb-interaction-dependent effect of high-order sideband generation in an optomechanical system. *Phys. Rev. A* **95**(3), 033820 (2017).
15. Si, L. G., Guo, L. X., Xiong, H. & Wu, Y. Tunable high-order-sideband generation and carrier-envelope-phase-dependent effects via microwave fields in hybrid electro-optomechanical systems. *Phys. Rev. A* **97**(2), 023805 (2018).
16. Xiong, H., Si, L. G., Lü, X. Y., Yang, X. & Wu, Y. Carrier-envelope phase-dependent effect of high-order sideband generation in ultrafast driven optomechanical system. *Opt. Lett.* **38**(3), 353–5 (2013).

17. Kong, C. et al. High-order sideband generation in a two-cavity optomechanical system with modulated photon-hopping interaction. *Laser Phy. Lett.* **15**(11), 115401 (2018).
18. He, B., Yang, L., Lin, Q. & Xiao, M. Radiation Pressure Cooling as a Quantum Dynamical Process. *Phys. Rev. Lett.* **118**, 233604 (2017).
19. Li, Y., Wu, L. A. & Wang, Z. D. Fast Ground-State Cooling of Mechanical Resonators with Time-dependent Optical Cavities. *Phys. Rev. A* **83**, 043804 (2011).
20. Nongthombam, R., Sahoo, A. & Sarma, A. K. Ground-state cooling of a mechanical oscillator via a hybrid electro-optomechanical system. *Phys. Rev. A* **104**(2), 023509 (2021).
21. Weis, S. et al. Optomechanically induced transparency. *Science* **330**(6010), 1520–1523 (2010).
22. Xiong, H., Si, L. G., Zheng, A. S., Yang, X. & Wu, Y. Higher-order sidebands in optomechanically induced transparency. *Phys. Rev. A* **86**(1), 013815 (2012).
23. Xiong, H. & Wu, Y. Fundamentals and applications of optomechanically induced transparency. *Appl. Phys. Rev.* **5**, 3 (2018).
24. Lü, H., Wang, C., Yang, L. & Jing, H. Optomechanically induced transparency at exceptional points. *Phys. Rev. Appl.* **10**(1), 014006 (2018).
25. Zhang, J. Q., Li, Y., Feng, M. & Xu, Y. Precision Measurement of Electrical Charge with Optomechanically Induced Transparency. *Phys. Rev. A* **86**, 053806 (2012).
26. Jing, H. et al. Optomechanically-induced transparency in parity-time-symmetric microresonators. *Sci. Rep.* **5**(1), 9663 (2015).
27. Lu, X. H., Si, L. G., Wang, B., Wang, X. Y. & Wu, Y. Tunable optomechanically induced transparency in a gain-assisted optomechanical system. *J. Phys. B: Atomic, Mol. Opt. Phys.* **52**(8), 085401 (2019).
28. Kronwald, A. & Marquardt, F. Optomechanically induced transparency in the nonlinear quantum regime. *Phys. Rev. Lett.* **111**(13), 133601 (2013).
29. Shahidani, S., Naderi, M. H. & Soltanolkotabi, M. Control and manipulation of electromagnetically induced transparency in a nonlinear optomechanical system with two movable mirrors. *Phys. Rev. A* **88**(5), 053813 (2013).
30. Ma, P. C., Zhang, J. Q., Xiao, Y., Feng, M. & Zhang, Z. M. Tunable double optomechanically induced transparency in an optomechanical system. *Phys. Rev. A* **90**, 043825 (2014).
31. Jiang, C. et al. Tunable transparency and amplification in a hybrid optomechanical system with quadratic coupling. *J. Phys. B: At. Mol. Opt. Phys.* **52**, 215402 (2019).
32. Hao, H. et al. Electromagnetically and optomechanically induced transparency and amplification in an atom-assisted cavity optomechanical system. *Phys. Rev. A* **100**(2), 023820 (2019).
33. Aplet, L. J. & Carson, J. W. A Faraday Effect Optical Isolator. *Appl. Opt.* **3**(4), 544 (1964).
34. Fang, K. J. et al. Generalized Non-reciprocity in an Optomechanical Circuit via Synthetic Magnetism and Reservoir Engineering. *Nat. Phys.* **13**, 465–471 (2017).
35. Khanikaev, A. B., Mousavi, S. H., Shvets, G. & Kivshar, Y. S. One-way Extraordinary Optical Transmission and Nonreciprocal Spoof Plasmons. *Phys. Rev. Lett.* **105**, 126804 (2010).
36. Fan, L. et al. An all-silicon passive optical diode. *Science* **335**(6067), 447–450 (2012).
37. Shadrivov, I. V., Fedotov, V. A., Powell, D. A., Kivshar, Y. S. & Zheludev, N. I. Electromagnetic wave analogue of an electronic diode. *New J. Phys.* **13**(3), 033025 (2011).
38. Nazari, F. et al. Optical isolation via PT-symmetric nonlinear Fano resonances. *Opt. Express* **22**(8), 9574 (2014).
39. Guo, X. X., Ding, Y. M., Duan, Y. & Ni, X. J. Nonreciprocal metasurface with space-time phase modulation. *Light Sci. Appl.* **8**(1), 123 (2019).
40. Estep, N. A., Sounas, D. L., Soric, J. & Alù, A. Magnetic-free non-reciprocity and isolation based on parametrically modulated coupled-resonator loops. *Nat. Phys.* **10**(12), 923–927 (2014).
41. Kang, M. S., Butsch, A. & Russell, P. S. J. Reconfigurable light-driven opto-acoustic isolators in photonic crystal fibre. *Nat. Photon.* **5**(9), 549 (2011).
42. Xu, X. W. & Li, Y. Optical nonreciprocity and optomechanical circulator in three-mode optomechanical systems. *Phys. Rev. A* **91**(5), 053854 (2015).
43. Tian, L. & Li, Z. Nonreciprocal quantum-state conversion between microwave and optical photons. *Phys. Rev. A* **96**, 013808 (2017).
44. Ruesink, F., Miri, M. A., Alu, A. & Verhagen, E. Nonreciprocity and magnetic-free isolation based on optomechanical interactions. *Nat. Commun.* **7**(1), 13662 (2016).
45. Shen, Z. et al. Experimental realization of optomechanically induced non-reciprocity. *Nat. Photon.* **10**(10), 657–661 (2016).
46. Miri, M. A., Ruesink, F., Verhagen, E. & Alù, A. Optical nonreciprocity based on optomechanical coupling. *Phys. Rev. Appl.* **7**(6), 064014 (2017).
47. Habraken, S. J. M., Stannigel, K., Lukin, M. D., Zoller, P. & Rabl, P. Continuous mode cooling and phonon routers for phononic quantum networks. *New J. Phys.* **14**, 115004 (2012).
48. Sliwa, K. M. et al. Reconfigurable Josephson Circulator/Directional Amplifier. *Phys. Rev. X* **5**, 041020 (2015).
49. Hafezi, M. & Rabl, P. Optomechanically induced non-reciprocity in microring resonators. *Opt. Express* **20**, 7672 (2012).
50. Kim, J., Kuzyk, M. C., Han, K., Wang, H. & Bahl, G. Non-reciprocal Brillouin scattering induced transparency. *Nat. Phys.* **11**, 275 (2015).
51. Dong, C. H. et al. Brillouin-scattering-induced transparency and non-reciprocal light storage. *Nat. Commun.* **6**, 6193 (2015).
52. Xiong, H., Si, L. G. & Yang, X. XWu. Y. Asymmetric optical transmission in an optomechanical array. *Appl. Phys. Lett.* **107**, 9 (2015).
53. Hatano, N. & Nelson, D. R. Localization transitions in non-Hermitian quantum mechanics. *Phys. Rev. Lett.* **77**(3), 570–573 (1996).
54. Longhi, S., Gatti, D. Della. & Valle, G. Non-Hermitian transparency and one-way transport in low-dimensional lattices by an imaginary gauge field. *Phys. Rev. B* **92**(9), 094204 (2015).
55. Shen, Y., Bradford, M. & Shen, J. T. Single-photon diode by exploiting the photon polarization in a waveguide. *Phys. Rev. Lett.* **107**(17), 173902 (2011).
56. Longhi, S., Gatti, D. Della. & Valle, G. Robust light transport in non-Hermitian photonic lattices. *Sci. Rep.* **5**(1), 13376 (2015).
57. Zhu, X. et al. Photonic non-Hermitian skin effect and non-Bloch bulk-boundary correspondence. *Phys. Rev. Res.* **2**(1), 013280 (2020).
58. Barzanjeh, S., Aquilina, M. & Xuereb, A. Manipulating the flow of thermal noise in quantum devices. *Phys. Rev. Lett.* **120**(6), 060601 (2018).
59. Malz, D. et al. Quantum-limited directional amplifiers with optomechanics. *Phys. Rev. Lett.* **120**(2), 023601 (2018).
60. Wang, D. Y. et al. Photon blockade in a double-cavity optomechanical system with nonreciprocal coupling. *New J. Phys.* **22**(9), 093006 (2020).
61. Spillane, S. M. et al. Ideality in a Fiber-Taper-Coupled Microresonator System for Application to Cavity Quantum Electrodynamics. *Phys. Rev. Lett.* **91**(4), 043902 (2003).
62. Guo, Y., Li, K., Nie, W. & Li, Y. Electromagnetically-induced-transparency-like ground-state cooling in a double-cavity optomechanical system. *Phys. Rev. A* **90**(5), 053841 (2014).
63. Ciuti, C. & Carusotto, I. Input-output theory of cavities in the ultrastrong coupling regime: The case of time-independent cavity parameters. *Phys. Rev. A* **74**(3), 033811 (2006).
64. Gardiner, C. W. *Zoller* (P. Quantum Noise, Springer Springer, 2004).

65. Manipatruni, S., Robinson, J. T. & Lipson, M. Optical Nonreciprocity in Optomechanical Structures. *Phys. Rev. Lett.* **102**, 213903 (2009).

Funding
The work was supported by the National Science Foundation of China (Grant No. 12105092) and the Hubei Province Natural Science Foundation innovation and development joint fund project (Grant No. 2024AFD010).

Declarations

Competing interest
The authors declare that there are no conflicts of interest related to this article.

Additional information
Correspondence and requests for materials should be addressed to C.K.

Reprints and permissions information is available at www.nature.com/reprints.

Publisher's note Springer Nature remains neutral with regard to jurisdictional claims in published maps and institutional affiliations.